SOLTZBERG, L. J., FAPPIANO, S. A., HIDEK, L. E., O'BRIEN, M. J. & SUAREZ, L. L. (1992). *Acta Cryst.* A48, 457–461.

SUNAGAWA, I. (1981). *Bull. Miner.* **104**, 81–87.

SUNAGAWA, I. (1987). In *Morphology of Crystals*, Part B, pp. 509–587, edited by I. SUNAGAWA. Boston: D. Reidel.

THOMPSON, D. (1961). *On Growth and Form*, abridged ed. by J. T. BONNER. Cambridge: Cambridge University Press.

THOMPSON, J. M. T. & STEWART, H. B. (1986). *Nonlinear Dynamics and Chaos*. New York: John Wiley.

WINCHELL, A. N. & WINCHELL, W. (1964). *The Microscopical Characters of Artificial Inorganic Solid Substances*, p 101. New York: Academic Press.

WYCKOFF, R. G. (1964). *Crystal Structures*, 2nd ed., Vol. 2, pp. 364–365. New York: Interscience.

Crystal Chemistry and Structures of Lead–Antimony Sulfides

BY ANICETA SKOWRON AND I. DAVID BROWN

*Institute for Materials Research, McMaster University, Hamilton, Ontario, Canada L8S 4M*1

Abstract

Using chemical and topological rules to describe the structural chemistry of Pb^{2+} and Sb^{3+}, we show that the substitution of Sb^{3+} into PbS (galena) results in four possible topological series of structures, and that the conflicting requirements of chemical bonding and charge neutrality severely limit the number of structures that can occur in each series. The model accounts for the existence of most of the compounds found in the pure Pb–Sb–S phase diagram. It correctly predicts the distribution of Pb^{2+} and Sb^{3+} over the various cation sites and shows why the mirror plane is lost in some phases.

1. Introduction

Lead and antimony are widely found in nature in the form of sulfides and many different mineral forms have been reported (Craig, Chang & Lees, 1973). Most of the minerals contain impurities and, in many cases, these impurities are important in stabilizing structures that would not be stable in the pure Pb–Sb–S system. For example, the plagionite group of minerals: semseyite, heteromorphite, plagionite and füllopite, which have also been obtained in hydrosynthesis experiments at temperatures near 673 K (Robinson, 1948; Jambor, 1968), fail to appear in the dry system. Heating experiments on natural and synthetic compounds of this group cause their decomposition to phases stable in the dry system. This may indicate, as suggested by Garvin (1973), that the plagionite group minerals contain an additional essential component, probably hydrogen, liberated during heating. In this paper, we confine ourselves to the dozen or so compounds known to occur in the pure ternary system.

The dry $PbS–Sb_2S_3$ system has been the subject of several experimental studies (Garvin, 1973; Craig *et al.*, 1973; Hoda & Chang, 1975; Salanci & Moh, 1970; Wang, 1976; Salanci, 1979; Bortnikov Nekrasov, Mozgova & Tsepin, 1981). Salanci (1979) has published a phase diagram, an adapted form of which, shown in Fig. 1, indicates six ternary compounds between PbS and Sb_2S_3: $II = Pb_7Sb_4S_{13}$, $III = Pb_3Sb_2S_6$, $IV = boulangerite$, $Pb_5Sb_4S_{11}$, $V =$
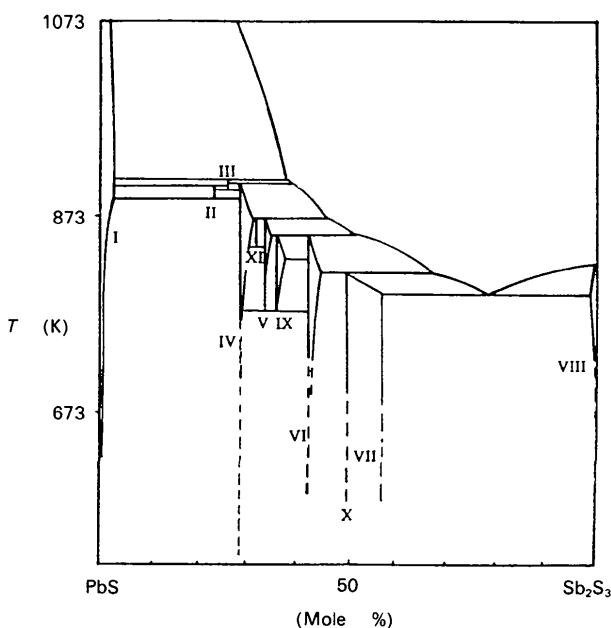

Fig. 1. Schematic phase diagram of the $PbS–Sb_2S_3$ system after Salanci (1979). The phases are I, galena; II, $Pb_7Sb_4S_{13}$; III, $Pb_3Sb_2S_6$; IV, boulangerite; V, $Pb_2Sb_2S_5$ (monoclinic); VI, robinsonite; VII, zinckenite; VIII, stibnite; IX, $Pb_5Sb_6S_{14}$; X, $PbSb_2S_4$; XI, $Pb_7Sb_6S_{16}$.

$Pb_2Sb_2S_5$, VI = robinsonite, $Pb_4Sb_6S_{13}$, and VII = zinckenite, $PbSb_2S_4$. Wang (1976) found that V has two polymorphs, one orthorhombic (V_o) and one monoclinic (V_m) and he reported two other compounds: $Pb_5Sb_6S_{14}$ (IX) and a compound with composition between $Pb_5Sb_6S_{14}$ and $Pb_2Sb_2S_5$. All these compounds melt incongruently and, apart from zinckenite, have relatively narrow and stoichiometric composition ranges. Three of them, boulangerite, robinsonite and zinckenite, are known as minerals. The crystal structures of eight of the ternary compounds have been reported and, together with Sb_2S_3, can be grouped into four homologous series (Table 1). The structural motifs of the four series are shown in Figs. 2(a)–(d).

In recent years, various authors have proposed schemes whereby the complex structures of these compounds are built up conceptually from rather simple parent motifs by various symmetry operations. For sulfides of As, Sb or Bi with Pb or Sn, this

approach has been used by Andersson & Hyde (1974), Takèuchi & Takagi (1974), Hyde, Bagshaw, Andersson & O'Keeffe (1974), Makovicky & Karup-Møller (1977a,b), Makovicky (1977) & Wuensch (1979), Makovicky & Hyde (1979, 1981) and Makovicky (1981, 1983, 1985a, 1994). Many of these schemes are rather complex and different authors have developed the structures in different ways. The approach used in this paper draws on the ideas presented in the above works, but with more emphasis on the chemical constraints on the structure. By doing so, we are able to predict which structures should form, how the cations are distributed among the various possible sites and the influence that this distribution has on the structure.

We first compare the structural chemistry of Pb^{2+} and Sb^{3+} (§2), then show how the galena structure of PbS (NaCl type) can be conceptually broken into ribbons (§3) which are reassembled under the constraints imposed by the structural chemistry (§§4–7).

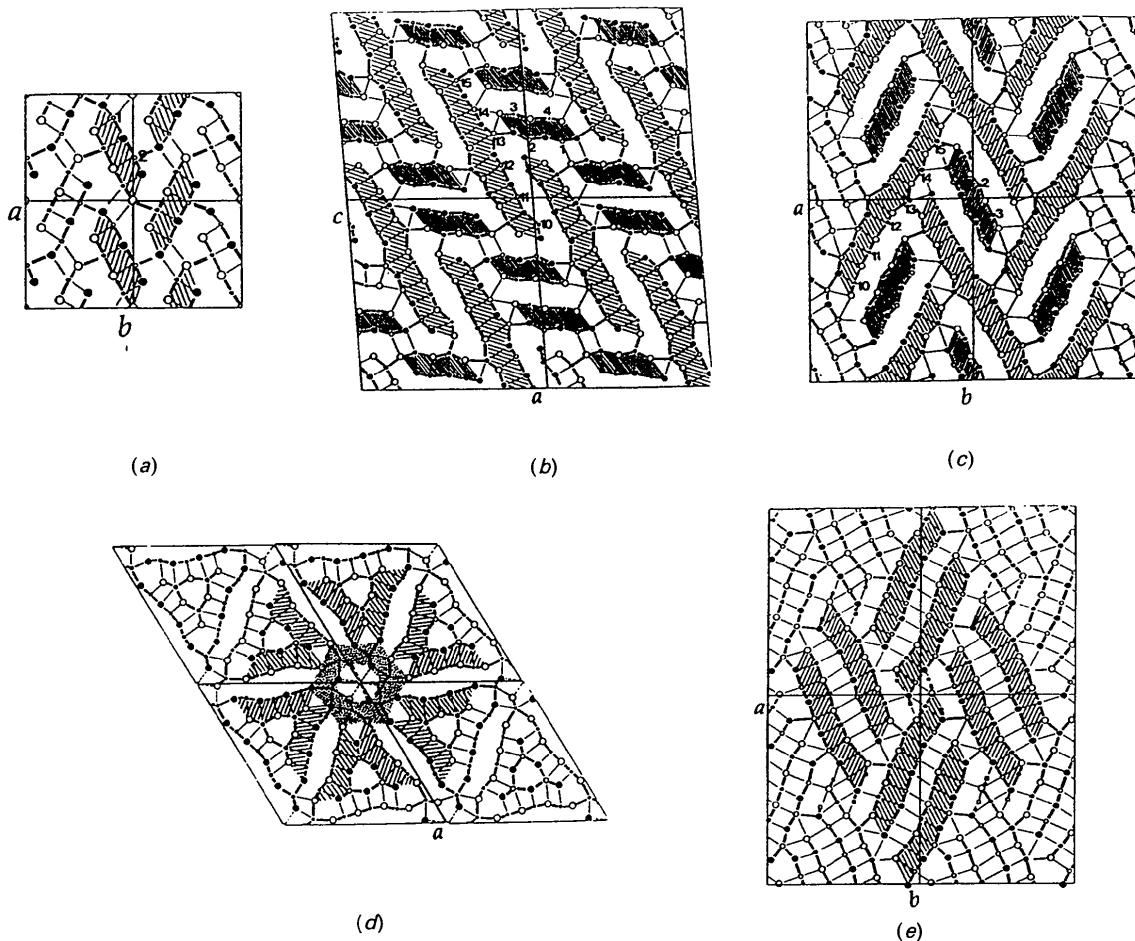(a)   (b)   (c)

(d)   (e)

Fig. 2. The crystal structure of (a) stibnite, (b) robinsonite, (c) boulangerite, (d) zinckenite and (e) cosalite projected down [001]. In order of decreasing size, the circles indicate S^2 , Pb^{2+} and Sb^{3+} ions. Ions at $z = 0.5$ and $z = 0.75$ are denoted as open and full circles. In (e) the sites indicated by squares are occupied by Cu^{2+}.

Table 1. *Reported* Pb–Sb–S *compounds*

The symbolic description given in columns 4 and 5 is explained in the text.

Name of the series	Phase	Formula	Symbol	Short symbol	References
Stibnite	VIII	Sb_2S_3	$R^4(1,1)-L^4(1,1)$	$s4/4$	Bayliss & Nowacki (1972)
	X	$PbSb_2S_4$	$R^6(1,1)-L^6(1,1)$	$s6/6$	Tilley et al. (1986), Smith & Hyde (1983)
	V_o	$Pb_2Sb_2S_5$	$R^8(1,1)-L^8(1,1)$	$s8/8$	Skowron & Brown (1990a), Skowron (1991)
	III	$Pb_3Sb_2S_6$	$R^{10}(1,1)-L^{10}(1,1)$	$s10/10$	Smith & Hyde (1983)
Robinsonite	VI	$Pb_4Sb_6S_{13}$	$R^{12}(2,2)-2L^4(1,0)$	$r12/4$	Petrova et al. (1978a), Skowron & Brown (1990b)
	IX	$Pb_5Sb_6S_{14}$	$R^{14}(2,2)-2L^4(1,0)$	$r14/4$	Skowron et al. (1992)
	XI	$Pb_7Sb_6S_{16}$	$R^{14}(2,2)-2L^6(1,0)$	$r14/6$	Wang (1976)
Boulangerite	IV	$Pb_5Sb_4S_{11}$	$R^{12}(2,2)-R^6(0,0)$	$b12/6$	Born & Hellner (1960), Petrova et al. (1978b), Skowron & Brown (1990c)
	II	$Pb_7Sb_4S_{13}$	$R^{14}(2,2)-R^8(0,0)$	$b14/7$	Skowron et al. (1994)
Zinckenite	VII	$PbSb_2S_4$			Portheine & Nowacki (1975)

Finally we explore the effect of the ribbon packing on the cation distribution and geometry (§8) and compare the predictions with observation (§§9–10).

2. Why Pb^{2+} is a stronger Lewis acid than Sb^{3+}

Wherein it is shown that, despite its larger charge, some of the bonds formed by Sb^{3+} are weaker than those formed by Pb^{2+}

Pb^{2+} and Sb^{3+} are both ions that contain a lone electron pair in their valence shell. According to the VSEPR theory (Gillespie & Hargittai, 1991), such ions should form coordination environments in which the lone pair occupies one of the bonding sites, giving, for six coordination, five bonds to the S atoms arranged in a square pyramid and one vacant site occupied by the lone pair. The axial bond is short and the metal atom lies slightly below the plane of the four equatorial ligand as shown in Fig. 3. In solids, one, two or occasionally three long (secondary) bonds are found lying close to the direction of the lone pair. Our discussion will focus on these
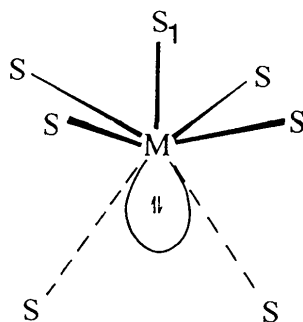

Fig. 3. Bonding around Pb^{2+} or Sb^{3+} with a stereoactive lone pair. The metal is seven-coordinated and the axial bond M—S_1 is the shortest with the lone electron pair and two secondary bonds opposite.

secondary bonds as they are the bonds responsible for the cohesion and packing in these compounds.

The steric effects of the lone pair are most pronounced for the elements lying near the top of the periodic table. The anisotropies become less marked in the heavier metals and Pb^{2+} can, in cases such as PbS (galena), be found in regular coordination in which the steric effects of the lone pair are completely suppressed. The environment of Sb^{3+}, which lies in the period above Pb^{2+}, is expected to be more distorted, and its secondary bonds are expected to be weaker, than those formed by Pb^{2+}. This difference can be quantified using the bond-valence model (Brown, 1992; Skowron & Brown, 1990b), which determines the strength or valence of a bond from its length. The valences of the axial and secondary bonds in Pb–Sb–S compounds are shown in Fig. 4 as a function of the Sb^{3+} content of the site. The circles show, for seven-coordinate cation sites, the sum of the bond valences found for the two secondary bonds. The crosses show the valences of the short axial bonds which are *trans* to the lone pair. As expected, the latter increase with the effective oxidation state of the cation, but the average valence of each of the two secondary bonds decreases from around $0.30/2 = 0.15$ v.u. (valence units) for Pb^{2+} to $0.04/2 = 0.02$ v.u. for Sb^{3+}. Thus, we have the paradox that the cation with the smaller charge (Pb^{2+}) forms the stronger secondary bonds. Increasing the Sb^{3+} content of a cation site in a crystal increases the effective charge of the cation at this site, but in order for this charge to result in stronger secondary bonds it is necessary to increase the proportion of Pb^{2+}. This paradox places strong restrictions on the kinds of compound that can be formed in the system since there will be only a limited value of the Pb^{2+}:Sb^{3+} ratio that can be accommodated at any given site. It is this limitation that results in only one or two members of each homologous series

being known. The effects of these are examined in detail in §6.

It is useful at this point to introduce the concept of Lewis acid strength, defined as the expected valence (or strength) of the bonds that a cation forms. In the following discussion, we will be particularly concerned with the secondary bonds. We, therefore, take the Lewis acid strength of Pb^{2+} to be 0.15 v.u. and that of Sb^{3+} to be 0.02 v.u. In addition, we can define the total Lewis acid strength of the cation as the sum of the Lewis acid strengths of all the secondary bonds it forms. The total Lewis acid strength of a cation is thus the cation's valence available for forming bonds external to the ribbon. When Pb^{2+} forms two secondary bonds, its total Lewis acid strength is $2 \times 0.15 = 0.30$ v.u. and when Sb^{3+} forms two secondary bonds, its total Lewis acid strength is 0.04 v.u. We also apply the term to the ribbon fragment introduced in the next section. The total Lewis acid strength of a ribbon is the sum of the total Lewis acid strengths of all the cations in the ribbon. Lewis base strengths can be similarly defined for atoms carrying negative charge (i.e. the S^{2-} ions). The usefulness of this definition lies in the valence-matching principle (Brown, 1992), which states that bonds will tend to form when the cation has a Lewis acid strength equal to the Lewis base strength of the anion. In the present case, Pb^{2+} will tend to bond to S^{2-} ions with a larger Lewis base strength (i.e. those with a larger residual charge) and Sb^{3+} will bond to S^{2-} ions with a smaller Lewis base strength.

3. How the building blocks (ribbons) of Pb–Sb–S compounds are formed from the galena structure

Wherein it is shown that the basic building blocks (ribbons) of the Pb–Sb–S *compounds are derived from the structure of galena* (PbS) *by allowing the lone electron pair to become stereoactive and partially substituting* Sb^{3+} *for* Pb^{2+}

The structures of solids in the Pb–Sb–S system can be conceptually derived from the galena (NaCl) structure of PbS by the following simple steps first proposed by Hofmann (1935) and extended by Hellner (1958) and Petrova, Pobedimskaya & Belov (1980).

The galena structure is first broken into (100) sheets, as shown by the broken lines in Fig. 5(a), in order to give the cations the square pyramidal coordination expected around atoms with stereoactive lone pairs. So that the secondary bonds linking the sheets can avoid the lone-pair direction, the sheets are sheared by half a cell along the galena [011] direction (perpendicular to the plane of Fig. 5 and corresponding to the short c axis in the Pb–Sb–S compounds), thereby replacing the single long bond by two secondary bonds and giving the ions a $5 + 2$ coordination. This is the structure found for Tl^I (Helmholtz, 1936), where the lone pair is expected to be stereochemically expressed, as pointed out by Makovicky (1985b).
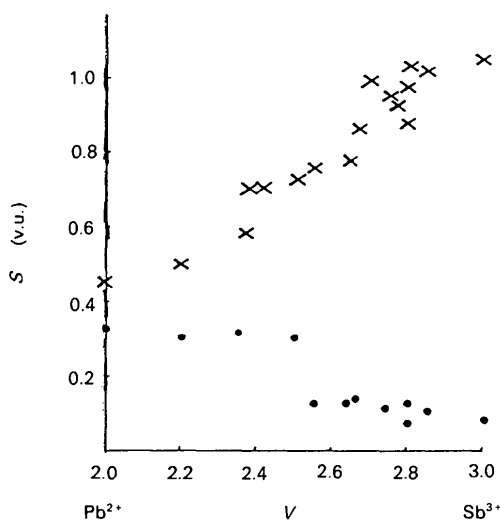

Fig. 4. The observed bond valences (s) versus the effective oxidation state (V) of the seven-coordinated cation sites in Pb–Sb–S compounds. The valences of the axial bonds are shown as crosses and the sum of the bond valences of the two secondary bonds opposite to the axial by dots. Bond valences are calculated from the bond lengths using r_o(Pb—S) = 2.451 and r_o(Sb—S) = 2.522 Å.
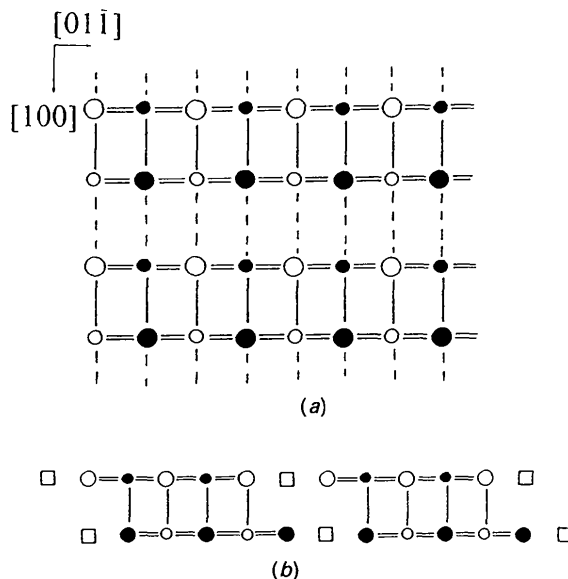

Fig. 5. (a) The crystal structure of galena (PbS) viewed down [011] and split into (100) sheets. The large circles represent S^{2-}, the small circles represent Pb^{2+}. Open and filled circles lie at different levels. The cations have square pyramidal coordination within the sheets. The sheets are linked only by long bonds. (b) Ordering of the cation vacancies splits the sheets into ribbons. The squares represent cation vacancies and the ribbons are extended perpendicular to the plane of the figure.

If Sb^{3+} is substituted for Pb^{2+}, three Pb^{2+} ions must be replaced by two Sb^{3+} ions plus a vacancy in order to maintain charge neutrality. If the vacancies are ordered, the sheets will break into ribbons as shown in Fig. 5(b). The width of the ribbons will depend on the proportion of Sb^{3+} present, the higher the concentration of Sb^{3+} the narrower the ribbon. The ribbons in the observed structures are infinitely extended along the galena [011] direction with a short repeat distance of 4 Å as shown in Fig. 6. All the structural variety in the series lies in the plane perpendicular to this axis. Consequently, the remainder of the discussion will be restricted to two dimensions. The structure will be displayed viewed down this short axis and the ribbon will be represented by a single repeat as shown in Fig. 5(b), corresponding to the formula unit of the ribbon.

It requires two vacancies (one on each face) to separate each ribbon from the sheet (Fig. 5b). Each ribbon thus contains four Sb^{3+} ions to give the composition $Sb_4S_6.nPbS = Sb_4Pb_nS_{n+6}$ for an electrically neutral ribbon. In principle, n can have any value but, as shown below, there are constraints that prevent it from becoming too large. In structures with two or more different ribbons, each individual ribbon need not be electrically neutral providing that the whole structure is neutral. The formula of a ribbon can more generally be written as

$$[Sb_{4+c}Pb_{N-4-c}S_{N+2}]^c, \qquad (1)$$

where N is the total number of cations in the ribbon and the charge, c, may be positive or negative.

4. How the ribbons bond to each other

Wherein it is shown that the principal bonding between the ribbons occurs from the Pb^{2+} ions on the face of one ribbon to the S^{2-} ions on the edge of the other,
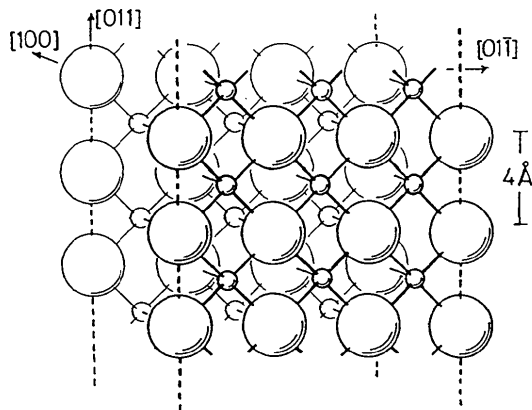

Fig. 6. A three-dimensional view of part of a ribbon. Directions are given relative to the galena unit cell.

and that the high charge but small Lewis acid strength of Sb^{3+} restricts the widths of the ribbons that can be formed

(1) shows that the ribbons may be positively or negatively charged depending on the relative amounts of Sb^{3+} and Pb^{2+} present. If only one kind of ribbon is present in the crystal, it must be electrically neutral and, therefore, contain exactly four Sb^{3+} ions combined with, in principle, any number of Pb^{2+} ions. If two different types of ribbon are present, they must have equal and opposite charge. Pauling's principle of parsimony suggests that structures with many different types of ribbon will not be found. For this reason, we assume that only structures with one or two different types of ribbon will occur.

The ribbons will be linked by Lewis acid–Lewis base bonds formed between the anions (S^{2-}) of one ribbon and the cations (Sb^{3+} and Pb^{2+}) of its neighbour. As is apparent from Fig. 5(b), the edges of the ribbons will always carry a negative charge since they consist only of S^{2-} ions which, since they form only two or three bonds to cations within the ribbon, will carry a larger unsatisfied negative charge than the five-coordinated S^{2-} ions on the faces. Since the strongest bonds will be formed between the strongest Lewis base (edge S^{2-}) and the strongest Lewis acid (Pb^{2+}), the principal cohesive force between ribbons will occur where the S^{2-} ions on the edge of one ribbon meet the Pb^{2+} ions on the face of another, forming an edge-to-face junction. Weaker bonds will also be formed between the weakly basic S^{2-} ions on the face of one ribbon and the weakly acidic Sb^{3+} ions on the face of an adjacent ribbon, forming a face-to-face junction. The ribbons will, therefore, arrange themselves in a tiling which provides for edge-to-face (Pb—S) and face-to-face (Sb—S) bonding, and the relative proportions of Pb^{2+} and Sb^{3+} present will depend on the relative amounts of each of these types of bonding. Note that edge-to-edge bonding will not occur as the edges contain only Lewis bases (S^{2-}). Even though the face-to-face bonds are important in determining the tilings of the ribbons, they are very weak and can be ignored in a quantitative analysis of the bond valences. We shall assume that the Lewis acid strength of a ribbon is contributed only by Pb^{2+} and the Lewis base strength only by S^{2-} on the edges.

The total Lewis acid strength, A, and the total Lewis base strength, B, of a ribbon measure the sum of the positive and negative charges, respectively, localized on the surface of the ribbon. The sum of A and B will, therefore, equal the net charge, c, on the ribbon (2)

$$A + B = c. \qquad (2)$$

B, by definition a negative number, is roughly con-

stant ranging between -0.8 and -1.2 v.u. The Lewis acid strength, however, will depend on the number of Pb^{2+} ions in the ribbon. From Fig. 4 we expect that $A \simeq 0.30$ v.u. × number of Pb^{2+} ions present.

Consider a ribbon whose faces bond only to the faces of other ribbons, i.e. a ribbon that does not bond to the edge of any neighbouring ribbon. We can designate this ribbon as $R(0,0)$, where the two integers in the parentheses give the number of edges bonding respectively to each of its two faces. Such a ribbon should contain no Pb^{2+} (since there are no edge-to-face junctions) and its faces should, therefore, carry no acid strength $(A = 0)$. However, the S^{2-} ions at the edge carry a base strength of -1.0 v.u. The ribbon should, following (2), have a charge of -1.0. (1) shows that such a ribbon will have the formula $Sb_3S_5^-$.

Consider now the ribbon $R(1,1)$, each of whose faces bond to one edge of a second ribbon. Fig. 7(c) shows that three bonds link the two S^{2-} ions on an edge to Pb^{2+} ions on a face. Assuming that each of the three bonds has a valence of 0.15 v.u., the total positive charge on each face will be $3 \times 0.15 = +0.45$ v.u., contributing a total charge of $+0.9$ v.u. when both faces are included. If the ribbon is neutral, each of the two edges will carry the complementary charge of -0.45 v.u. Such ribbons contain three Pb^{2+} ions (1.5 on each face) and, according to (1), will have the composition $Sb_4Pb_3S_9$.

In order to meet the charge and bonding requirements as the ribbon is further widened, there must be one Sb^{3+} ion (to provide one extra unit of charge) for every three Pb^{2+} ions (to provide the locations on the surface for the charge to reside). So, to widen the ribbons while maintaining a $Pb^{2+}:Sb^{3+}$ ratio consistent with these requirements, it is necessary to add $SbPb_3S_4^+$. Widening the uncharged $Sb_4Pb_3S_9$ ribbons by adding one such unit gives $Sb_5Pb_6S_{13}^+$. The six Pb^{2+} ions will form 14 bonds to the edges of adjacent ribbons, requiring that two edges bond to each face as shown in Fig. 7(d).* These ribbons can be described as $R(2,2)$. Increasing the width further by adding a second unit gives $Sb_6Pb_9S_{17}^{2+}$, requiring three edges to bond to each face $[R(3,3)]$. Most triple edge-to-face arrangements require tilings with at least three distinct types of ribbon and are, therefore, not expected to occur. The exception is a tiling in which an $R(0,0)$ ribbon is sandwiched between two $R(3,0)$ ribbons, all three ribbons having the same width. Such an arrangement is not possible since the $R(3,0)$ ribbons would have to be at least 12 cations wide in order to form a triple junction and no $R(0,0)$ ribbon is known wider than ten cations.

* In real structures, two of the six Pb^{2+} ions are found to form three instead of two external bonds, i.e. they are eight-coordinate as shown in Fig. 7(d). This coordination will be assumed in all our discussions of the arrangements with two edges bonding to a face, an arrangement later referred to as a double junction.

(a)   (b)

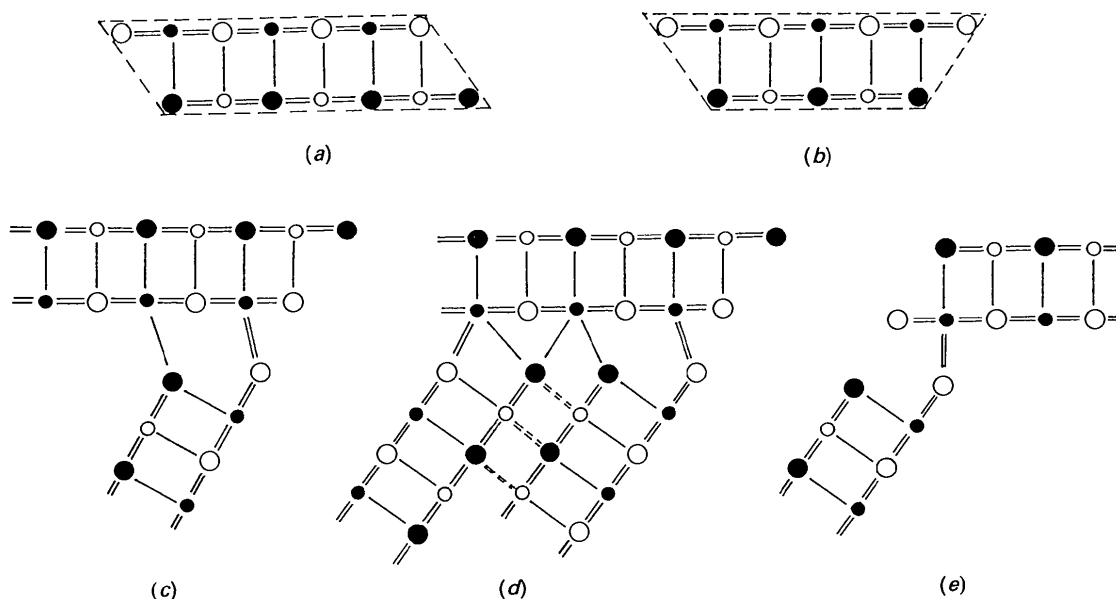(c)   (d)   (e)

Fig. 7. Ribbons with (a) even and (b) odd numbers of cations per unit repeat (even and odd ribbons) viewed down the c axis. The cross section of an even ribbon is a 60° parallelogram, while that of an odd ribbon is a 60° trapezium. (c)–(e) Edge-to-face junctions of ribbons. In (c) one ribbon joins to another ribbon through three bonds of valence 0.15 v.u. each (a single junction), in (d) two ribbons join to another ribbon through eight bonds (double junction). (e) Bonding of a ribbon edge to the acute end of a ribbon face brings the strongly basic S^{2-} ions too close.

Table 2. *Ideal ribbon types*

These ribbons are the only ones that obey (2), where each Pb^{2+} ion contributes ca 1/3 v.u. to the Lewis acid strength. The numbers in parentheses refer to the number of edges bonding to each of the faces of the ribbon. The ribbons indicated by *, and other ribbon types not included in the table, cannot be incorporated in tilings with less than three distinct types of ribbon.

Label	Composition	Width	Charge
R(0,0)	Sb_3S_5	3	−1.0
R(1,0)	$Sb_{3.5}Pb_{1.5}S_7$	5	−0.5
R(1,1)	$Sb_4Pb_3S_9$	7	0
R(2,0)	$Sb_4Pb_3S_9$	7	0
R(2,1)*	$Sb_{4.5}Pb_{4.5}S_{11}$	9	0.5
R(2,2)	$Sb_5Pb_6S_{13}$	11	1.0
R(3,3)*	$Sb_6Pb_9S_{17}$	15	2.0

Table 2 lists the characteristics of the ideal ribbons described above. For topological reasons discussed below, not all the chemically possible ribbons can exist in real structures. In particular, as shown in the next section, it is not possible to pack ribbons with odd numbers of cations. This, in practice, rules out all the ideal ribbons listed in Table 2. However, it is usually possible to substitute some Pb^{2+} onto the Sb^{3+} sites (or *vice versa*), allowing for some variation in the compositions and charges shown in Table 2, as discussed in the next section, but the further the composition differs from these ideal values, the more unstable the ribbon becomes.

5. How the ribbons pack together

Wherein it is shown that only four tilings are possible for even ribbons and none for odd ribbons

Exploring the different ways in which the ribbons can pack together to form three-dimensional structures is a problem in two-dimensional tiling. We assume three conditions that the tilings must satisfy.

Rule 1. The tiling of the ribbons must fill space.

Rule 2. The Lewis acid sites (Pb^{2+}) must be concentrated in the region of the edge-to-face junctions.

Rule 3. The facing parts of parallel ribbons must be sheared to ensure that the face-to-face ($Sb^{3+}—S^{2-}$) bonds avoid the lone-pair direction.

If all the ribbons have the same orientation designated as R, all will be parallel, resulting in edge-to-edge connections of the type shown in Fig. 5(b). These are not expected to occur since they bring the strongly basic S^{2-} ions together. Therefore, it is necessary for the ribbons to occur in at least two different orientations, labelled R and L. In the plane perpendicular to the ribbon axis, ribbons with an even number of cations have a cross section that is a 60° parallelogram as shown in Fig. 7(a), those with an odd number of cations have a cross section that is a 60° trapezium shown in Fig. 7(b). Odd and even ribbons, therefore, form different tilings, which it is convenient to discuss separately.

5.1. Tilings with odd ribbons

Odd ribbons, having a trapezium as cross section, can pack in three orientations which we label R, L and T. The ribbons will form triangles as shown in Fig. 8(a). However, examination of the edge-to-face junction shown in Fig. 7(c) shows that the three trapezia cannot be related by a threefold axis because each is displaced by c/2 with respect to its two neighbours. Thus, closed figures, such as that shown in Fig. 8(a) can only occur if they contain an even number or ribbons. Further, as shown in Fig. 7(e), edge-to-face junctions cannot occur at acute corners as this brings strongly basic S^{2-} ions into contact without providing any suitable Pb—S bonds. The long face, being bounded by acute corners must,

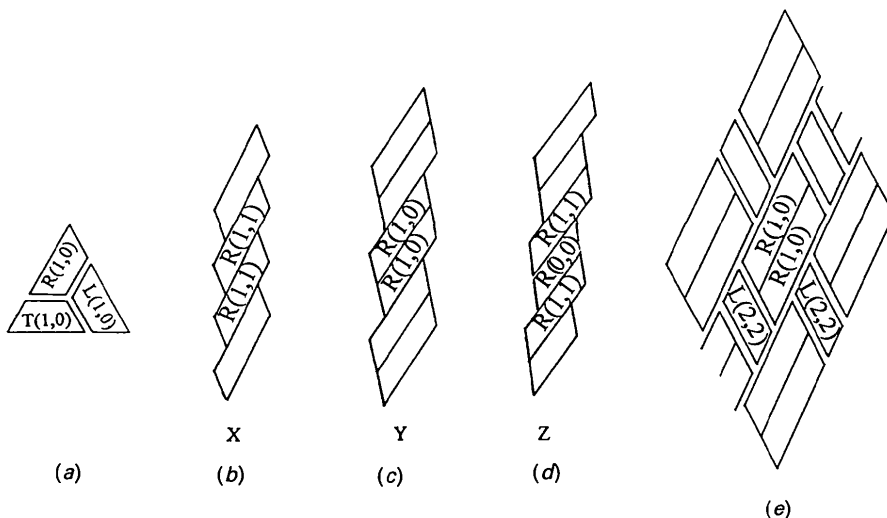(a)   (b)   (c)   (d)

X   Y   Z

(e)

Fig. 8. (a) A triangular packing of three odd ribbons. (b)–(d) The three types of stacking of parallel ribbons that can form single and double junctions through their edges. (e) A tiling with edges forming a junction to the middle of a face.

therefore, pack with another long face, which does not lead to space-filling tiling. For these two reasons no tiling is possible with odd ribbons.

5.2. Tilings with even ribbons

The 60° angle between adjacent sides of the parallelogram requires that edge-to-face bonded ribbons pack at 60° to one another. Therefore, at least two ribbon orientations, R and L inclined at 60° to each other, are required, with the edges of the L ribbons bonding to the faces of the R ribbons and vice versa.
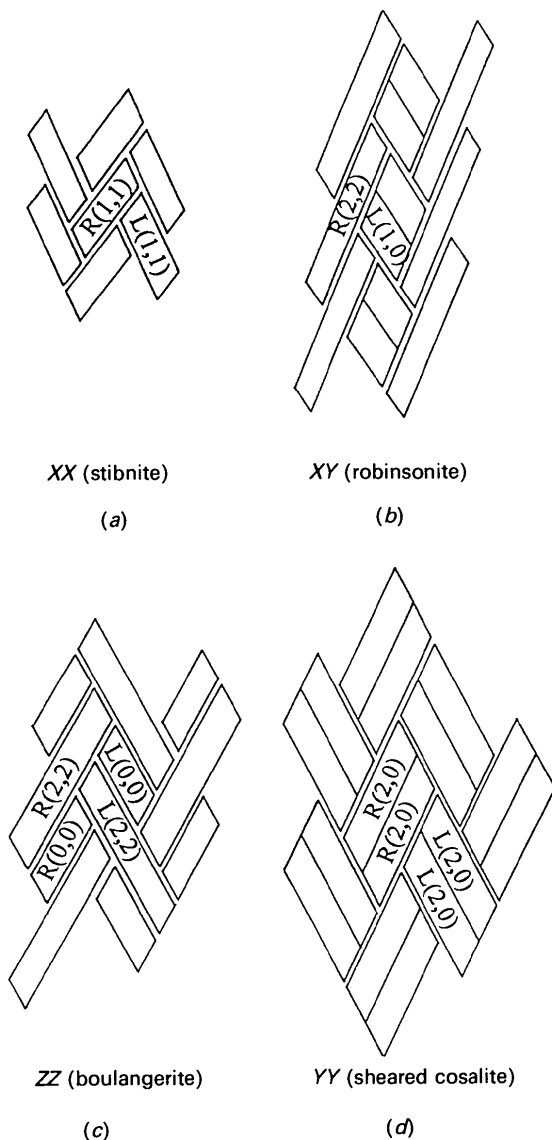

XX (stibnite) XY (robinsonite)

(a) (b)

ZZ (boulangerite) YY (sheared cosalite)

(c) (d)

Fig. 9. Space-filling tilings constructed from the stacks X, Y and Z. The shown ribbons are close to their ideal size. Comparison with Fig. 2 shows that XX tiling corresponds to stibnite, XY to robinsonite and ZZ to boulangerite arrangement. The XY tiling is similar to that present in cosalite shown in Fig. 2(e).

The face-to-face bonding between the R ribbons will result in the R ribbons forming stacks of the types illustrated in Figs. 8(b)–(d). The L ribbons will form similar stacks. For reasons noted above, in drawing Figs. 8(b)–(d) we assumed that the edge-to-face bonds will only occur at the obtuse corner of the long edge of the parallelogram. Tilings in which the edges bond to the centres of faces are conceptually possible, but they impose impossible restrictions on the chemistry. In the tiling shown in Fig. 8(e), for example, the $L(2,2)$ ribbons would have the formula $Pb_6S_8^{4-}$, which would require a negative charge of at least -2 on each edge.

Labelling the three possible stacks shown in Figs. 8(b)–(d) as X, Y and Z, the only tilings that fill space are XX, YY, XY and ZZ, shown in Fig. 9. XZ and YZ are excluded because they involve at least three different types of ribbon.

6. How chemical constraints limit the size of the ribbons

Wherein the chemical constraints are summarized by a set of five rules

In addition to the three topological rules given in the previous section, there are five chemical conditions which must also be satisfied. These are given as rules which can be expressed mathematically. Rules 4 to 6 are obeyed exactly, rules 7 and 8 need only be obeyed approximately.

Rule 4. The charge on the ribbon (c) is determined by its composition

The relationship between the net charge, c, carried by a ribbon having a total of N cation sites, of which N_{Pb} contain Pb^{2+} and N_{Sb} contain Sb^{3+}, can be obtained from (1)

$$N_{Sb} = 4 + c,$$ (3a)

and

$$N_{Pb} = N - 4 - c.$$ (3b)

Rule 5. The total Lewis acid strength, A, plus the total Lewis base strength, B, of a ribbon equals the charge, c, (2)

$$A_R + B_R = c_R.$$ (2)

Note that the base strength, B, is negative and the subscript R refers to ribbon R. A similar equation occurs for ribbon L.

Rule 6. The total acid strength of the R ribbons equals the total base strengths of the L ribbons and vice versa

This is expressed by (4), which can be derived from (2) by setting the total charge of all ribbons equal to

zero and recognizing that the acid parts of one ribbon bond to the base parts of the other and *vice versa*

$$n_R A_R = -n_L B_L \qquad (4a)$$

$$n_L A_L = -n_R B_R, \qquad (4b)$$

where n_R and n_L are the numbers of R and L ribbons in the formula unit, respectively.

Rule 7. The total acid strength of a ribbon is given by its Pb^{2+} content and the types of junction it forms

We assume to a first approximation that, as shown in Fig. 4, each seven-coordinated Pb^{2+} ion contributes 0.3 v.u. to the total acid strength of the ribbon and the Sb^{3+} ions make no contribution. For eight-coordinated Pb^{2+} (see footnote) we assume that the coordination polyhedron is essentially regular with each bond having a valence of 2/8 v.u. The contribution of such Pb^{2+} ions to the total acid strength is then $3 \times 2/8 = 0.75$ v.u.

The total Lewis acid strength of a ribbon containing N_{Pb} Pb^{2+} ions, all of which are seven-coordinated (*i.e.* the ribbon forms only single junctions, shown in Fig. 7c), is $A = 0.3N_{Pb}$. Where the ribbon forms a double junction (Fig. 7d), one of the Pb^{2+} ions is found to be eight-coordinate. In this case the total Lewis acid strength of the ribbon is increased by $0.75 - 0.30 = 0.45$ v.u. for every double junction. Therefore, in general, the total Lewis acid strength of a ribbon can be written as

$$A = 0.30N_{Pb} + 0.45N_D, \qquad (5)$$

where N_D is the number of double junctions formed by the ribbon. Substituting for N_{Pb} in (5) from (3b) and rearranging using (2) yields

$$A = 0.23(N - B + 1.50N_D - 4). \qquad (6)$$

Substitution of (6) into (2) gives the corresponding net charge on the ribbon (7)

$$c = -1.69 + 0.23N + 0.35N_D. \qquad (7)$$

From this equation, one can see that any ribbon with $N > 7$ must be positive, *i.e.* it must have more Sb^{3+} than a corresponding neutral ribbon, and any ribbon with $N < 4$ must be negative, *i.e.* it must have more Pb^{2+} than a corresponding neutral ribbon. In between the charge will depend on the number of double junctions. Except, therefore, for structures composed of electrically neutral ribbons with $N = 6$–7, we expect to find structures composed of negatively charged narrow ribbons having $N < 6$ cations combined with positively charged wide ribbons with $N > 7$.

Since the acid strength of a ribbon is a measure of the strength of its external bonds, Pb^{2+} will concentrate at the cation sites which lie at the edge-to-edge

junctions between the ribbons. A maximum of two Pb^{2+} ions can be accommodated in a single junction and three in a double junction, regardless of the width of the ribbon. Thus, the maximum acid strength a junction can have is the strength it has when these sites are fully occupied by Pb^{2+}, namely $A^{max} = 0.6$ v.u. for a single junction and $A^{max} = 1.35$ v.u. for a double junction. The maximum total acid strength for a ribbon can thus be written as

$$A^{max} = 0.60N_s + 1.35N_D, \qquad (8)$$

where N_s is the number of single junctions and N_D is the number of double junctions. (8) places an upper limit on the values of A that can be found using (6).

Rule 8. The non-junction cation sites may contain up to 50% Pb^{2+}

Increasing the ribbon width while keeping the charge constant requires that the Pb^{2+} content of the ribbon also increases. Quite quickly the number of Pb^{2+} ions in the ribbon becomes larger than the number needed to fill the sites at the junctions, and A, as calculated from (5), will exceed A^{max}. It will only be possible to increase the width of the ribbons further if Pb^{2+} can be placed in non-junction sites. This will strengthen the face-to-face bonding between the ribbons, but we ignore such bonds in our definition of the Lewis acid strength of the ribbon. Therefore, the Pb^{2+} content of a ribbon can exceed that required to provide the total Lewis acid strength. If a structure has, say, up to 50% Pb^{2+} substituted on an Sb^{3+} site, (5) will give a value for A which is too large, but the limit on the Pb^{2+} content can be calculated by recognizing that the value of (5) cannot exceed $A^{max} + 0.15N_n$, *i.e.*

$$A^{max} + 0.15N_n \geq 0.30N_{Pb} + 0.65N_D, \qquad (9a)$$

where 0.15 is the contribution of a half-filled Pb^{2+} non-junction site to the acid strength [according to (5)] and N_n is the number of non-junction sites capable of accepting Pb^{2+}.

These include all the sites except those that form junctions and the two sites at the acute corner of each ribbon. The latter are normally occupied only by Sb^{3+} because Pb^{2+} cannot form strong enough bonds to the terminal S^{2-} ions. Hence

$$A^{max} \geq A' = A - 0.15(N - 2 - 2N_s - 3N_D). \qquad (9b)$$

7. Predicting which compounds can be formed in the Pb–Sb–S system

Wherein it is shown that the chemical constraints in rules 4–8 restrict the widths of the ribbons that can be found in each of the four possible tilings.

Rules 1–3 define the geometries of the four allowed tilings, rules 4–8, summarized by (6), (8) and

(9), permit us to predict the widths of the ribbons that will be stable for each of these tilings. For convenience, we shall refer to the tilings by the name of the principal representative Pb–Sb–S compound having that tiling. The tilings are shown in Fig. 9 and their structures in Fig. 2. Stibnite (Fig. 2a) is the archetype of the structures that adopt the XX tiling, robinsonite (Fig. 2b) that of the XY tiling and boulangerite (Fig. 2c) that of the ZZ tiling. No Pb–Sb–S structure is known which adopts the XY tiling, but cosalite (Srikrishnan & Nowacki, 1974) has a similar structure in which the pairs of face-sharing ribbons are not sheared (Fig. 2e). We refer, therefore, to XY as the 'sheared cosalite' structure.

7.1. Stibnite series (XX tiling)

In the XX tiling, the $R(1,1)$ and $L(1,1)$ ribbons are joined by single junctions, as shown in Fig. 9(a). Labelling the ribbons so that $N_R \geq N_L$, and eliminating B using (4) with $n_R = 1$ and $n_L = 1$, (6), (8) and (9b) reduce to

$$A_R = 0.24N_R + 0.06N_L - 1.21 \qquad (10a)$$

$$A^{max} = 1.20 \qquad (10b)$$

$$A' = A - 0.15(N - 6). \qquad (10c)$$

These equations are plotted in Fig. 10(a) for $N_R = N_L$. The ideal composition, i.e. the composition of the most stable compound, lies at the intercept of the A and A^{max} lines ($N_R = 8$), for here the junction sites are exactly filled with Pb^{2+}. Some additional Pb^{2+} can be placed on Sb^{3+} sites corresponding to positions along the A^{max} line, but only as far as the intersection with A'. The presence of excess Sb^{3+} occupying the Pb^{2+} sites corresponds to positions along the A line, the limit being reached when $A = 0$ (no Pb^{2+} present in the structure). The allowed compounds are shown with a heavy line and the further their composition lies from the ideal composition, the less stable they are. If we represent the compound by $R^N(1,1)-L^N(1,1) = sN/N$, where s indicates the stibnite series and N indicates the ribbon widths, Fig. 10(a) indicates that structures $R^4(1,1)-L^4(1,1) = s4/4$ to $R^{10}(1,1)-L^{10}(1,1) = s10/10$ are possible with $R^8(1,1)-L^8(1,1) = s8/8$ being the most stable.

Similar plots for $N_R > N_L$ and $N_L = 4, 6, 8...$ predict that $s6/4$ to $s12/4$, $s8/6$ to $s10/6$ and $s10/8$ are also possible. All the four predicted members of the series with $N_R = N_L$ have been reported, but none with $N_R > N_L$. The observed acid strengths of the ribbons in $s4/4$ (VIII) and $s8/8$ (V), indicated as squares in Fig. 10(a), are close to those predicted by the model.

7.2. Robinsonite series (XY tiling)

In the XY tiling, there is one $R(2,2)$ for every two $L(1,0)$ ribbons joined by double and single junctions on their faces as shown in Fig. 9(b). The R ribbon must be at least eight cations wide if it is to form double junctions, hence, topologically $N_R \geq 8$ and the ribbon will carry a positive charge. The L ribbon must, therefore, carry a negative charge which restricts $N_L \leq 6$. Since $N_R > N_L$ and recognizing that in (4) $n_R = 1$ and $n_L = 2$, (6), (8) and (9b) take the form given in (11a)–(11f)

$$A_R = 0.24N_R + 0.12N_L - 0.68 \qquad (11a)$$

$$A_L = 0.24N_L + 0.03N_R - 1.03 \qquad (11b)$$

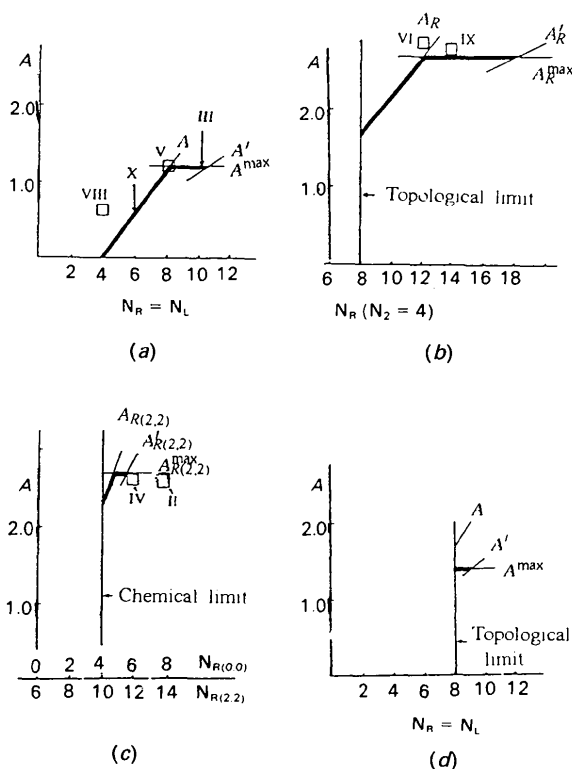$$A_R^{max} = 2.70 \qquad (11c)$$

(a)

(b)

(c)

(d)

Fig. 10. (a) Plot of equations 10(a)–10(c) for the stibnite series (XX tiling), where $N_R = N_L$. Structures with $N = 4$–10 are possible with $N = 8$ being the most stable. The observed acid strength for compounds with $N = 4$ and 8 are indicated by the squares. (b) Plot of equations 11(a)–11(f) for the robinsonite series (XY tiling). $N_L = 4$ and values of N_R between 8 and 18 are possible. The observed acid strengths for $N_R = 12$ and 14 are indicated as squares. (c) Plot of equations 13(a)–13(c) for the boulangerite series (ZZ tiling). $N = 10$ should exist and $N = 12$ is predicted to be marginally stable. The squares indicate the observed A for the structures with $N = 12$ and 14. (d) Plot of $L(a)$–(c) for the sheared cosalite series (YY tiling). The tiling requires that for both ribbons, $N_R = N_L \geq 8$. Only $N = 8$ is allowed.

$$A_L^{max} = 0.60 \qquad (11d)$$

$$A_R' = A_R - 0.15(N_R - 8) \qquad (11e)$$

$$A_L' = A_L - 0.15(N_L - 4). \qquad (11f)$$

The acidity of the R ribbons is shown in Fig. 10(b) as a function of N_R for $N_L = 4$.

For $N_L = 4$, the most stable structure will occur for $N_R = 12$, the structure for robinsonite (VI), but any value between 8 and 18 should be possible. The observed acid strengths of the wider ribbons of $R^{12}(2,2)$–$2L^4(1,0) = r12/4$ (VI) and $R^{14}(2,2)$–$2L^4(1,0) = r14/4$ (IX) are shown as squares in Fig. 10(b). For $N_L = 6$, N_R can lie in the range 8–16 with 12 being the most stable value.

7.3. Boulangerite series (ZZ tiling)

In the ZZ tiling, Fig. 9(c), there are two different R ribbons [$R(2,2)$ and $R(0,0)$] and two different L ribbons [$L(2,2)$ and $L(0,0)$]. Since we have assumed that only two chemically distinct ribbons occur, $R(2,2)$ and $L(2,2)$ must be identical, as must $R(0,0)$ and $L(0,0)$. Therefore, it is only necessary to consider the $R(2,2)$ and $R(0,0)$ ribbons.

The tiling requires that as the width of one ribbon increases, the width of the other must increase by the same amount (12)

$$N_{R(2,2)} - N_{R(0,0)} = 6. \qquad (12)$$

Solving (6), (8) and (9b) using (12) and a suitably modified form of (4) yields (13a)–(13f)

$$A_{R(2,2)} = 0.56N_{R(2,2)} - 3.29 \qquad (13a)$$

$$A_{R(2,2)}^{max} = 2.70 \qquad (13b)$$

$$A_{R(2,2)}' = A_{R(2,2)} - 0.15[N_{R(2,2)} - 8] \qquad (13c)$$

$$A_{R(0,0)} = 0.23[N_{R(0,0)} - B_{R(0,0)} - 4] = 0 \qquad (13d)$$

$$A_{R(0,0)}^{max} = 0 \qquad (13e)$$

$$A_{R(0,0)}' = A_{R(0,0)} - 0.15[N_{R(0,0)} - 2]. \qquad (13f)$$

$A_{R(2,2)}$ is plotted against $N_{R(2,2)}$ and $N_{R(0,0)}$ in Fig. 10(c). Since base strengths are taken to be negative, (13d) yields $N_{R(0,0)} \geq 4$, hence $N_{R(2,2)} \geq 10$. According to Fig. 10(c) only $R^{10}(2,2)$–$R^4(0,0) = b10/4$ should exist with $b12/6$ (IV) being possibly stable. The former compound is not known but the latter is the stable compound boulangerite and the next member of the series, $R^{14}(2,2)$–$R^8(0,0) = b14/8$ (II), is also known. The observed boulangerite structures have longer chains than our simple rules predict, corresponding to excess Pb^{2+} content. The reason for this is discussed in §8. The observed acid strengths of the

wider ribbons in $b12/6$ (IV) and $b14/8$ (II) are indicated as squares in Fig. 10(c).

7.4. Sheared cosalite series (YY tiling)

In YY tiling, the $R(2,0)$ and $L(2,0)$ ribbons are joined by double junctions as shown in Fig. 9(d) and, again assuming $N_R \geq N_L$, (6), (8) and (9b) reduce to (14a)–(14c)

$$A_R = 0.24N_R + 0.06N_L - 0.75 \qquad (14a)$$

$$A^{max} = 1.35 \qquad (14b)$$

$$A' = A - 0.15(N - 5). \qquad (14c)$$

These equations are plotted in Fig. 10(d) for $N_R = N_L$. Because of the double edge-to-face junctions, the tiling in this structure requires both ribbons to be at least eight cations wide, indicated by the vertical line. The only possible structure with the YY tiling is $R^8(2,0)$–$L^8(2,0) = c8/8$. This is close to the limit of stability and is not likely to be observed for reasons discussed in §9 below.

8. How the cation distribution in the ribbons affects the geometry and stability

Wherein it is shown that the distribution of Pb^{2+} *and* Sb^{3+} *over the cation sites causes the ribbons to curl, and that the strain introduced by straightening them leads to the loss of the mirror plane and additional substitution of* Pb^{2+} *into the* Sb^{3+} *sites*

The rules in the previous section allow one to predict the distribution of Pb^{2+} and Sb^{3+} atoms over the different cation sites within a ribbon. The agreement between predicted and observed site occupation numbers, shown in Table 3 and Fig. 11, [(obs − calc)$_{rms}$ = 0.16], is quite satisfactory given the uncertainty in the measurements. Because Pb^{2+} is needed to form the face-to-edge junctions, it is concentrated in the faces near the obtuse corner of the ribbon while Sb^{3+} concentrates on the opposite side. This arrangement causes the ribbons to curl, since the Pb—S bonds on one face are longer than the Sb—S bonds on the opposite face (Fig. 12a). The effect will be larger for double junctions, which require three Pb^{2+} ions, than for single junctions that require only two. Curled ribbons do not pack well but, in order to straighten them, the bonds in the Sb^{3+} face must be stretched and those in the Pb^{2+} face compressed, leaving the atoms on the Sb^{3+} side underbonded (bond-valence sums less than the atomic valence) and those on the Pb^{2+} side to be overbonded. In order to relieve this strain, the compressed Pb^{2+} face buckles, with Pb^{2+} moving outward towards the neighbouring ribbon edge and S^{2-} moving inwards to form stronger bonds with the

Table 3. *Observed and predicted cation distribution in Pb–Sb–S compounds*

Composition	Symbol	Predicted occupations (% Sb)		Observed occupations (% Sb)
Stibnite series (XX)				
Sb_2S_3	$R^4(1,1)$–$L^4(1,1)$	M(1)	100	100
		M(2)	100	100
$PbSb_2S_4$	$R^6(1,1)$–$L^6(1,1)$	M(1)	100	Not known
		M(2)	50	
		M(3)	50	
$Pb_2Sb_2S_5$	$R^8(1,1)$–$L^8(1,1)$	M(1)	100	100
		M(2)	100	82
		M(3)	0	10
		M(4)	0	8
$Pb_3Sb_2S_6$	$R^{10}(1,1)$–$L^{10}(1,1)$	M(1)	100	Not known
		M(2)	50	
		M(3)	50	
		M(4)	0	
		M(4)	0	
Robinsonite series (XY)				
$Pb_4Sb_6S_{13}$	$R^{12}(2,2)$–$2L^4(1,0)$	M(1)	100	80
		M(2)	0	18
		M(3)	100	100
		M(4)	100	100
		M(10)	100	100
		M(11)	100	80
		M(12)	100	78
		M(13)	0	0
		M(14)	0	0
		M(15)	0	36
$Pb_5Sb_6S_{14}$	$R^{14}(2,2)$–$2L^4(1,0)$	M(1)	100	55
		M(2)	0	10
		M(3)	100	100
		M(4)	75	100
		M(10)	100	100
		M(11)	75	80
		M(12)	75	70
		M(13)	75	65
		M(14)	0	0
		M(15)	0	0
		M(16)	0	20
Boulangerite series (ZZ)				
$Pb_5Sb_4S_{11}$	$R^{12}(2,2)$–$R^6(0,0)$	M(1)	100	70
		M(2)	33	30
		M(3)	33	38
		M(10)	100	100
		M(11)	67	100
		M(12)	67	56
		M(13)	0	0
		M(14)	0	0
		M(15)	0	0
$Pb_7Sb_4S_{13}$	$R^{14}(2,2)$–$R^8(0,0)$	M(1)	100	M(1) 100
		M(2)	22	M(2) 28
		M(3)	22	M(3) 17
		M(4)	22	M(4) 14
		M(10)	100	M(10) 100
		M(11)	44	M(11) 65
		M(12)	44	M(12) 36
		M(13)	44	M(13) 40
		M(14)	0	M(14) 0
		M(15)	0	M(15) 0
		M(16)	0	M(16) 0

(Skowron, Corbett, Boswell & Taylor, 1994). The tensile strain on the Sb^{3+} side is relieved in two ways. Firstly, more Pb^{2+} can substitute for the smaller Sb^{3+} than is allowed by rule 8, thereby increasing the stability of the Pb^{2+}-rich phases, and, secondly, Sb^{3+} can move away from the centre of its coordination sphere according to the prediction of the distortion theorem (Brown, 1992). The only off-centre displacement that does not affect the bonding around the neighbouring cations is a displacement that breaks the mirror plane characteristic of so many of these structures. This accounts for some of the anomalies observed in the wider $R(2,2)$ ribbons of the boulangerite and robinsonite series, anomalies such as the loss of the mirror plane in the boulan-
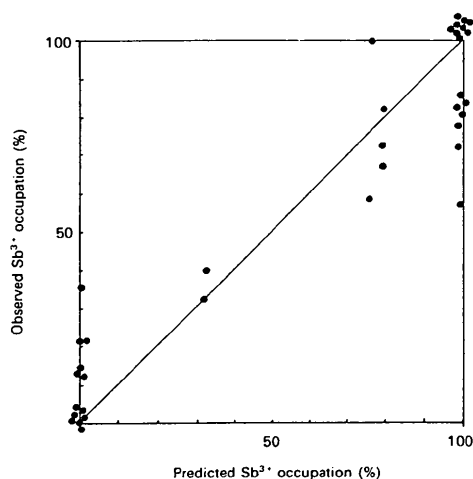
Fig. 11. Predicted and observed Sb^{3+} occupation of the cation sites in the Pb–Sb–S compounds.

(a)

(b)
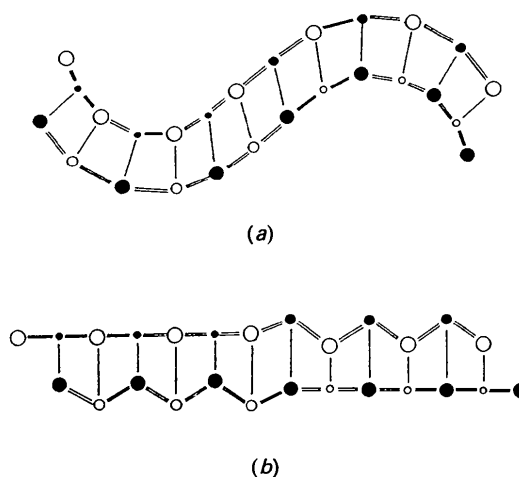
Fig. 12. (a) A ribbon showing the curling (exaggerated) produced by the required distribution of Pb^{2+} and Sb^{3+}. (b) The result of the strain introduced when the ribbon is straightened. In order of decreasing size, the circles indicate S^{2-}, Pb^{2+} and Sb^{3+} ions.

underbonded Sb^{3+} on the opposite face (Fig. 12b). Although this reduces the under- and over-bonding at the cations, it increases it for S^{2-}, a phenomenon that has been observed in a number of structures

gerite phase, $II = b14/6$, and possibly also in the robinsonite phase, $IX = r14/4$, and the unusual stability of the higher (Pb-rich) homologues of boulangerite. A similar increase in stability would be expected for the Pb-rich members of the robinsonite series, but these compounds will not be observed for reasons discussed in the next section.

9. How well have we done?

Wherein it is shown that we can correctly predict most of the compounds in the Pb–Sb–S *phase diagram, as well as their structures and relative stabilities*

Table 4 lists all the predicted structures arranged by structural series with the most stable structures underlined. The observed structures are indicated in the last column. Table 5 gives the same list ordered by composition (vertically) and approximate relative stability (horizontally). The stabilities have been estimated qualitatively from the graphs shown in Fig. 10, allowing for the tendency of the uncurling strain to stabilize higher Pb^{2+} concentrations in $R(2,2)$ ribbons. Table 5 lists 14 compositions in the Pb–Sb–S system that correspond to predicted structures. For some compositions, several structures are predicted and, in these cases, the structure predicted to be most stable is the one observed. Further, the predicted stabilities correspond roughly to the existence ranges observed in the phase diagram (Fig. 1), the more stable structures occurring over a wider temperature range. The clustering of the compositions listed in Table 5, particularly in the 20–30% range, agrees with the general features of the phase diagram. Notable are the large regions in the Pb- and Sb-rich regions where ternary compounds are neither predicted nor observed.

(I) *Galena*

Galena stands at the beginning of the series and is the model on which the other structures are based.

(II) $Pb_7Sb_4S_{13}$

This structure, $b14/8$, is stabilized only by the uncurling strain and has quite a small existence range in the phase diagram.

(III) $Pb_3Sb_2S_6$

Predicted only to be moderately stable, this compound, $s10/10$, also has a limited existence range.

$Pb_8Sb_6S_{17}$

A robinsonite homologue, $r16/6$, is predicted to be marginally stable at this composition. It has not been observed perhaps because it will have only a small

Table 4. *Predicted and observed* Pb–Sb–S *structures arranged by structure type*

Those predicted to be the most stable are in bold type.

Tiling	Series	Composition % Sb	Short symbol	Observed homologues
XX	Stibnite,	100	s4/4	VIII
	sNR/NL,	50	s6/6	X
	$R^{NR}(1,1)-L^{NL}(1,1)$	33	**s8/8**	V_o
		25	s10/10	III
		67	s6/4	—
		50	**s8/4**	—
		40	s10/4	—
		33	s12/4	—
		40	s8/6	—
		33	s10/6	—
		29	s10/8	—
XY	Robinsonite,	60	r8/4	—
	rNR/NL,	50	r10/4	—
	$R^{NR}(2,2)-2L^{NL}(1,0)$	43	**r12/4**	VI
		38	r14/4	IX
		33	r16/4	—
		30	r18/4	—
		43	r8/6	—
		38	r10/6	—
		33	r12/6	—
		30	**r14/6**	XI
		27	r16/6	—
ZZ	Boulangerite,	40	b10/4	—
	bN1/N2	29	**b12/6**	IV
	$R(2,2)^{N1}R(0,0)^{N2}$	27	b14/8	II
YY	Sheared cosalite,	33	c8/8	—
	cNR/NL			
	$R^{NR}(2,0)-L^{NL}(2,0)$			
	Zinckenite	50	—	VII

existence range and is very close to the composition of the much more stable boulangerite.

(IV) *Boulangerite*

Two structures are possible with this composition, the observed structure of boulangerite = $b12/6$ being clearly more stable than the structure in the stibinite series, $s10/8$, which is not known.

(XI) $Pb_7Sb_6S_{16}$

Wang (1976) reports a compound at this composition that has the correct unit cell for the $r14/6$ structure in the robinsonite series. However, this structure has yet to be confirmed.

(V) $Pb_2Sb_2S_5$

Six different predicted structures have this composition and two are expected to be relatively stable. The only confirmed structure is the orthorhombic member of the stibinite series, $s8/8$, but Wang also reports a monoclinic polymorph whose structure is unknown. The only compound with a sheared cosalite structure is predicted to have this composition. Given the number of competing structures with higher stability, it is clear why no members of this series have been observed.

Table 5. *Predicted compounds and structures arranged by composition*

Those observed are shown in bold type and are also listed in Table 1 where the references can be found. The symbols refer to the structural series stibnite (*s*), robinsonite (*r*), boulangerite (*b*), and sheared cosalite (*c*), the numbers refer to the widths of the ribbons.

	Observed			Predicted (short symbol)		
% Sb	Phase	Composition	Other	Most stable	Stable	Least stable
0	I	PbS	**Galena**			
22	II	$Pb_7Sb_4S_{13}$			**b14/8**	
25	III	$Pb_3Sb_2S_6$			**s10/10**	
27		$Pb_8Sb_6S_{17}$	•		r16/6	
29	IV	$Pb_5Sb_4S_{11}$		**b12/6**		s10/8
30	XI	$Pb_7Sb_6S_{16}$		**r14/6**		r18/4
33	V$_o$	$Pb_2Sb_2S_5$		**s8/8**	r16/4	c8/8
				r12/6		s10/6
						s12/4
38	IX	$Pb_3Sb_6S_{14}$		**r14/4**	r10/6	
40		$Pb_3Sb_4S_9$			b10/4	s8/6
					s10/4	
43	VI	$Pb_4Sb_6S_{13}$		**r12/4**		r8/6
50	VII	$PbSb_2S_4$	**Zinckenite**	r10/4		
	X			s8/4	**s6/6**	
60		$Pb_2Sb_6S_{11}$				r8/4
67		$PbSb_4S_7$				s6/4
100	VIII	Sb_2S_3				s4/4

(IX) $Pb_5Sb_6S_{14}$

Two structures are predicted for this composition, both in the robinsonite series. The more stable of the two, r14/4, is that observed.

$Pb_3Sb_4S_9$

It is surprising that no compound has been observed at this composition, given that we predicted two moderately stable structures in the boulangerite and stibinite series.

(VII) *Zinckenite*

Three structures are predicted by our model, but the observed structure is zinckenite, which is constructed on a different principle from the series we discuss in this paper. Zinckenite contains a sixfold axis, close to which the atoms can be disordered. This allows zinckenite to have a relatively wide composition range and may account for its stability. A member of the stibinite series predicted to be moderately stable, s6/6, has been seen in the electron microscope but is not known as a macroscopic crystal.

$Pb_2Sb_6S_{11}$ and $PbSb_4S_7$

Both these compositions are predicted to be marginally stable, the first in the robinsonite series, the second in the stibinite series. Neither is known.

(VIII) *Stibinite*

The final member of the series is, according to our model, only marginally stable. This reflects the deviations between the bonding properties of Sb in the observed stable Sb_2S_3 and the simple assumptions of our model.

10. Concluding remarks

Our model predicts the existence of four homologous series of Pb–Sb–S compounds, each with a limited number of stable structures. Not all of these structures will be observed because many of them have the same composition and only the most stable structure at each composition will appear in the phase diagram. Of the 12 ternary compounds that we predict, eight are known, though one of these, zinckenite, has a structure that belongs to the galena-derived structures of a differently defined type to those described here (Makovicky, 1985c). The remaining four compounds are not expected to be very stable and may either not exist or have such a limited existence field that they have so far been missed. Our model accounts for the distribution of Pb^{2+} and Sb^{3+} over the various cation sites and shows how this distribution can lead to strains in structures with double junctions that both stabilize the Pb-rich phases and lower the crystallographic symmetry.

The chief value of our approach lies not in the absolute precision with which it makes predictions since, necessarily, simplifications are made, but rather in the way in which it shows that chemical as well as topological constraints limit the number of possible structures. These constraints are expressed as a number of rules which not only allow us to understand the main features of the phase diagram, but also to account for much of the detailed geometry of the structures.

References

ANDERSSON, S. & HYDE, B. G. (1974). *J. Solid State Chem.* **9**, 92–101.

BAYLISS, P. & NOWACKI, W. (1972). *Z. Kristallogr.* **135**, 308–315.

BORN, L. & HELLNER, E. (1960). *Am. Mineral.* **45**, 1266–1271.

BORTNIKOV, N. S., NEKRASOV, I. Y., MOZGOVA, N. N. & TSEPIN, A. I. (1981). *Neues Jahrb. Mineral. Abh.* **143**, 37–60.

BROWN, I. D. (1992). *Acta Cryst.* **B48**, 553–572.

CRAIG, J. R., CHANG, L. L. Y. & LEES, W. R. (1973). *Can. Mineral.* **12**, 199–206.

GARVIN, P. L. (1973). *Neues Jahrb. Mineral. Abh.* **118**, 235–267.

GILLESPIE, R. J. & HARGITTAI, I. (1991). *The VSEPR Model of Molecular Geometry.* New York: Prentice Hall.

HELLNER, E. (1958). *J. Geology,* **66**, 503–525.

HELMHOLTZ, L. (1936). *Z. Kristallogr.* **95**, 129–137.

HODA, S. N. & CHANG, L. L. Y. (1975). *Can. Mineral.* **13**, 388–393.

HOFMANN, W. (1935). *Z. Kristallogr.* **92**, 161–173.

HYDE, B. G., BAGSHAW, A. N., ANDERSSON, S. & O'KEEFFE, M. (1974). *Annu. Rev. Mater. Sci.* **4**, 43–52.

JAMBOR, J. L. (1968). *Can. Mineral.* **9**, 507–521.

MAKOVICKY, E. (1977). *Neues Jahrb. Mineral. Abh.* **131**, 187–207.

MAKOVICKY, E. (1981). *Fortschr. Mineral.* **59**, 137–190.

MAKOVICKY, E. (1983). *Proc. NATO Adv. Study Inst. Ser. E,* **83**, 159–169.

MAKOVICKY, E. (1985a). *Neues Jahrb. Mineral. Abh.* **160**, 269–297.

MAKOVICKY, E. (1985b). *Fortschr. Mineral.* **63**(1), 45–89.

MAKOVICKY, E. (1985c). *Z. Kristallogr.* **173**, 1–23.

MAKOVICKY, E. (1994). *Eur. J. Mineral.* In the press.

MAKOVICKY, E. & HYDE, B. G. (1979). *Am. Inst. Phys. Conf. Proc.* **53**, 99–101.

MAKOVICKY, E. & HYDE, B. G. (1981). *Struct. Bonding,* **46**, 101–170.

MAKOVICKY, E. & KARUP-MØLLER, S. (1977a). *Neues Jahrb. Mineral. Abh.* **130**, 264–287.

MAKOVICKY, E. & KARUP-MØLLER, S. (1977b). *Neues Jahrb. Mineral. Abh.* **131**, 56–82.

PETROVA, I. V., KAPLUNNIK, L. N., BORTNIKOV, N. S., POBEDIMSKAYA, E. A. & BELOV, N. V. (1978a). *Dokl. Akad. Nauk SSSR,* **241**, 88–90.

PETROVA, I. V., KUZNETZOV, E. L., BELKONEVA, A. M., SIMONOV, E. A., POBEDIMSKAYA, E. A. & BELOV, N. V. (1978b). *Dokl. Akad. Nauk SSSR,* **242**, 337–340.

PETROVA, I. V., POBEDIMSKAYA, YE, A. & BELOV, N. V. (1980). *Miner. Zh.* **2**, 3–10.

PORTHEINE, J. C. & NOWACKI, W. (1975). *Z. Kristallogr.* **141**, 79–96.

ROBINSON, S. C. (1948). *Econ. Geol.* **43**, 293–312.

SALANCI, B. (1979). *Neues Jahrb. Mineral. Abh.* **135**, 315–326.

SALANCI, B. & MOH, G. H. (1970). *Neues Jahrb. Mineral. Abh.* **112**, 63–95.

SKOWRON, A. (1991). PhD thesis. McMaster Univ., Canada.

SKOWRON, A. & BROWN, I. D. (1990a). *Acta Cryst.* **C46**, 534–536.

SKOWRON, A. & BROWN, I. D. (1990b). *Acta Cryst.* **C46**, 527–531.

SKOWRON, A. & BROWN, I. D. (1990c). *Acta Cryst.* **C46**, 531–534.

SKOWRON, A., BROWN, I. D. & TILEY, R. D. J. (1992). *J. Solid State Chem.* **97**, 199–211.

SKOWRON, A., CORBETT, J. X., BOSWELL, F. & TAYLOR, N. (1994). *J. Solid State Chem.* In the press.

SMITH, P. P. K. & HYDE, B. G. (1983). *Acta Cryst.* **C39**, 1498–1502.

SRIKRISHNAN, T. & NOWACKI, W. (1974). *Z. Kristallogr.* **140**, 114–136.

TAKÈUCHI, Y. & TAKAGI, J. (1974). *Proc. Jpn Acad.* **50**, 76–79.

TILLEY, R. D. J., WRIGHT, A. C. & SMITH, D. J. (1986). *Proc. R. Soc. London Ser. A,* **408**, 9–22.

WANG, N. (1976). *Neues Jahrb. Mineral. Abh.* **128**, 167–175.

WUENSCH, B. J. (1979). *Am. Inst. Phys. Conf. Proc.* **53**, 337–354.

A Comparative Structural Study of a Flux-Grown Crystal of $K_{0.86}Rb_{0.14}TiOPO_4$ and an Ion-Exchanged Crystal of $K_{0.84}Rb_{0.16}TiOPO_4$

BY P. A. THOMAS

Department of Physics, University of Warwick, Coventry CV4 7AL, England

R. DUHLEV

Clarendon Laboratory, University of Oxford, Parks Road, Oxford OX1 3PU, England

AND S. J. TEAT

Department of Physics, University of Warwick, Coventry CV4 7AL, England

Abstract

The crystal structures of a flux-grown crystal, $K_{0.86}Rb_{0.14}TiOPO_4$, and an Rb/Ba ion-exchanged $KTiOPO_4$ crystal, $K_{0.84}Rb_{0.16}TiOPO_4$, are refined and compared. Both crystals are isostructural with potassium titanyl phosphate, $KTiOPO_4$. In both crystals, Rb substitutes for K only on the K(2) site with the crystallographically distinct K(1) site being solely occupied by K. However, in the ion-exchanged